Article

Investigations of self-heating effects in Silicon-Photomultipliers

Erika Garutti [*] , Stephan Martens , Joern Schwandt , Carmen Villalba-Pedro

Article

Investigations of Self-Heating Effects in Silicon-Photomultipliers

Erika Garutti *[ID], **Stephan Martens, Joern Schwandt** [ID] **and Carmen Villalba**

Institute for Experimental Physics, University of Hamburg, Luruper Chaussee 149, 22761 Hamburg, Germany
* Correspondence: erika.garutti@uni-hamburg.de, carmen.villabla@desy.de; Tel.: +49-40-8998-3779 (E.G.)

Abstract: The main consequence of radiation damage on a Silicon-Photomultiplier (SiPM) is a significant increase in the dark current. If the SiPM is not adequately cooled, the power dissipation causes it to heat up, which in turn affects its performance because of the increased temperature. To investigate this heating effect, experiments were carried out using a KETEK SiPM glued on an Al_2O_3 substrate, as well as HPK SiPMs that were either glued onto an Al_2O_3 substrate or a flexible PCB. The assemblies were connected either directly to a temperature-controlled chuck on a probe station, or through layers of materials with well-defined thermal resistance. An LED operated in DC-mode was used to illuminate the SiPM, and the resulting SiPM current was measured to determine the steady-state temperature. This temperature depended on the power dissipated in the multiplication region of the SiPM and the thermal resistance. This information can be utilized to adjust the SiPMs working point, taking into account the effects of self-heating. Similarly, this approach can be applied to packaged SiPMs that have an unknown thermal contact to a heat sink.

Keywords: SiPM; radiation damage; self-heating

1. Introduction

Silicon Photomultipliers (SiPMs) are the detector of choice for numerous applications in high-energy physics, astroparticle physics and space research, medical imaging, and societal applications. The operating conditions in these applications largely vary, e.g. temperatures can range from cryogenic [1] to 100 °C. Usually, the devices are operated in the dark, and visible photons are the signal to be detected, but in applications such as LiDAR systems (Light Detection and Ranging), SiPMs need to be operated in the presence of ambient light background [2,3]. At collider experiments, SiPMs are operated in a harsh radiation environment. The principal effect of radiation damage already at moderate fluences of $\Phi_{eq} = 10^{10}$ cm^{-2} is an increase of dark current [4,5]. For the Phase 2 Upgrade the CMS collaboration at LHC plans two new detectors equipped with SiPMs [6]. In the High Granularity Calorimeter (HGCAL) plastic scintillator tiles with SiPM readout will equip the rear active layers which, during the detector lifetime will accumulate a 1 MeV neutron equivalent fluence $\Phi_{eq} = 5 \cdot 10^{13}$ cm^{-2} [7]. Even worse will be the operation condition in the barrel MIP Timing Detector (MTD) which will reach a fluence of $\Phi_{eq} = 2 \cdot 10^{14}$ cm^{-2} [8]. Understanding the SiPM's response after radiation exposure is crucial for these applications. While the dark count rate (DCR) of non-irradiated SiPMs is typically in the range of 10-500 kHz/mm when operating in a dark environment at room temperature, it has been shown that the DCR increases by five orders of magnitude to above GHz/mm after a fluence $\Phi_{eq} = 10^{13}$ cm^{-2} even with cooling to -30 °C [8–11]. The same high (photo-)current is registered by SiPMs operated with background ambient light. These elevated currents result in significant power dissipation, potentially causing a rise in the SiPM temperature, an effect known as self-heating.

To maintain stable SiPM temperatures in such high dark count rate conditions, it is crucial to ensure a small thermal resistance between the SiPM and the heat sink [12]. Efficient heat dissipation is necessary to prevent self-heating and subsequent variations in the breakdown voltage of the SiPM, which changes its performance parameters such as gain and photon detection efficiency.

This research seeks to devise a method for gauging the temperature increase in SiPM caused by the dissipation of power in its amplification layer.

The SiPM's performance depends on the temperature T. The photocurrent measured at a constant bias voltage and photon rate decreases with increasing temperature, expressed as $I_{\text{photo}} \propto PDE(T) \cdot G(T) \cdot ECF(T)$, where PDE is the photodetection efficiency, G is the gain, and ECF is the excess charge factor [13]. The temperature sensitivity of the $PDE \propto FF \cdot QE(\lambda) \cdot P_{Geiger}(V_{\text{bias}}, T)$ is introduced via the voltage-dependent Geiger-breakdown probability, P_{Geiger}, with FF the device fill factor, and QE the wavelength-dependent quantum efficiency. An increase of T reduces the carriers' velocity due to increased scattering on the lattice. The ionization coefficients for holes and electrons decrease with T. Consequently, P_{Geiger} at a fix V_{bias} decreases, and the breakdown voltage, V_{bd} increases. An increase in V_{bd} with temperature leads to a decrease in gain, described by the relation: $G = C_{\text{pix}} \cdot (V_{\text{bias}} - V_{\text{bd}}(T))/q_0$.

In the study by Lucchini et al. [14], a method is proposed to evaluate the heating of SiPMs in various package configurations and to evaluate changes in temperature during operation at elevated dark count rates. The SiPM current (I_{SiPM}) is measured under constant illumination, and changes in T_{SiPM} are inferred from alterations in I_{SiPM} when the bias voltage is changed or the thermal conditions are changed by the air flow from a fan. This paper uses a similar approach for deducing temperature variations from current measurements. However, in our method, which we have introduced in [15], I_{SiPM} is measured in a cycle at a constant bias voltage while varying the intensity of light. This prevents abrupt variations in the SiPM working condition and parameters (G, PDE, ENF). The primary assumption underlying our analysis is that I_{SiPM} under constant illumination is solely dependent on $V_{\text{bias}} - V_{\text{bd}}(T)$. As part of this study, we crosscheck that both methods, Lucchini and ours, measure a consistent temperature increase in the SiPM, independently if the power increase is induced by a light intensity or a bias voltage increase.

The investigated SiPMs and the setup are described in Sect. 2. The analysis method and its application to determine the increase in SiPM temperature are explained in Sect. 4. The main results are given in Sect. 5, followed by the conclusions in Sect. 6.

2. SiPMs investigated and experimental setup

Two types of SiPMs were investigated. First, an R&D SiPM from KETEK [16] type MP15V09, with $V_{\text{bd}} = (27.60 \pm 0.02)$ V at 25 °C [17], pixel size of $15 \times 15 \ \mu m^2$, and number of pixels $N_{\text{pix}} = 27367$. The active region is circular with a radius $r_{\text{SiPM}} = 1.4$ mm. This SiPM is manufactured on a 700 μm thick silicon wafer and does not have a specially manufactured entrance window. The bare silicon sensor is glued on an alumina (Al_2O_3) substrate, with area $20 \times 25 \ mm^2$ and thickness 0.6 mm. The second sample is produced by Hamamatsu Photonics K.K. (HPK) [18] MPPC S14160-9769, with an active area of $3.0 \times 3.0 \ mm^2$, pixel size $10 \times 10 \ \mu m^2$, number of pixels: 89600 and $V_{\text{bd}} = (38.19 \pm 0.02)$ V at 25 °C. It is delivered as a surface-mount package with a silicon resin and glass-epoxy entrance window and has an overall thickness of 0.8 mm. This sample is tested both soldered on a flexible PCB, and on the same alumina as the KETEK sample to compare the different substrates. The information is summarised in Table 1.

Table 1. Summary information of the two SiPM models used in this study.

Sample ID	S6	S14160-9769
Manufacturer	KETEK	HPK (MPPC)
# pixels	27367	89600
Pixel size [µm]	15	10
Active area [mm^2]	6.2	3.0×3.0
Sample thickness [µm]	700	800
Substrate	Alumina	PCB/Alumina
V_{bd} (@25 °C) [V]	27.6	38.2
V_{bd} (@−30 °C) [V]	-	36.3
dV_{bd}/dT [mV K^{-1}]	22.4	33.5 (RT)
dV_{bd}/dT [mV K^{-1}]	-	31.3 ($\sim$ low T)
S_{photo} [%/K](@25 °C)	0.46% (10.4 OV)	0.69% (6.8 OV)
S_{photo} [%/K](@−30 °C)	-	0.60% (7.7 OV)

The current of the samples, mounted on a temperature-controlled chuck ($\Delta T \approx 0.1$ K), is measured using probe needles connected to a Keithley 6517B voltage source/current meter [19]. The alumina or PCB substrate is fastened to the chuck using a vacuum pump. For good thermal contact, the substrate is placed directly on the surface of the chuck. To emulate a degraded thermal contact of the SiPM, two polyoxymethylene (POM) layers of different thicknesses (1.5 and 3.0 ±0.1 mm) are placed between the substrate and the cold chuck, increasing the thermal resistance. The thermal conductivity of POM $k = 0.3$ W m^{-1} K^{-1} is close to that of commercially available PCB materials. The thermal contact between POM and Al2O3/HPK-housing is simply via an air-gap and may not be optimal. Three temperature sensors (PT-100) glued with a thermal foil are used. Two sensors record the temperature on the surface of the substrate, T_{sensor1} and T_{sensor2}, and a third that of the chuck, T_{sensor3}, according to the sketch of Figure 1.

The illumination is provided with light of a wavelength $\lambda = 470$ nm from an LED operated in DC mode, and surrounded by a diffuser. The setup is located in a light-tight and electrically shielded box.
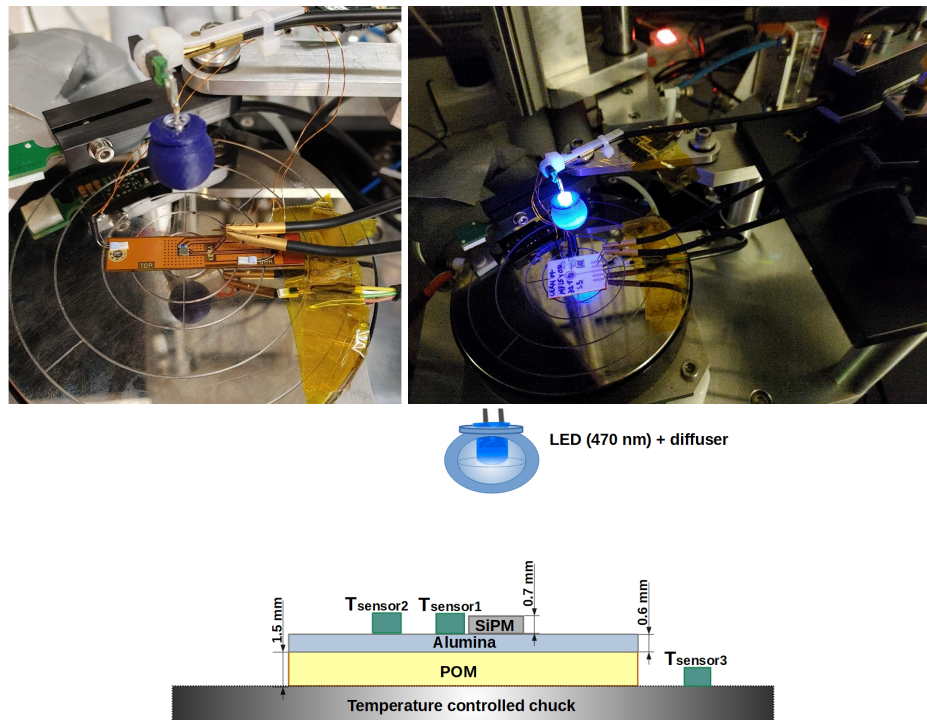
Figure 1. Photos and schematic of the experimental setup. Layout on the probe station: KETEK SiPM glued on the alumina substrate, with a POM layer to degrade the thermal contact with the chuck. The distances of the T_{sensors} on the alumina from the SiPM center are (3.2 ± 0.1) mm (T_{sensor1}) and (7.4 ± 0.1) mm (T_{sensor2}). The alumina substrate is depicted on the right, on the left is the PCB substrate.

3. Method

Two sets of data are recorded. The calibration data set, with the substrate in direct contact with the chuck, $I_{\text{cal}}(V_{\text{bias}}, T_{\text{chuck}}, I_{\text{LED}})$ is taken at several LED intensities, I_{LED}, with V_{bias} ranging from below V_{bd} to about 10 V overvoltage (OV), and T_{chuck} varied in five steps of 2.5 °C centred at 25 °C and −30 °C respectively. From the calibration data, the sensitivity function described in Sec. 4 is extracted. The sensitivity function is applied to the second set of data, the measurement cycle, used to determine the increase in the SiPM temperature from its measured current, in conditions with good and degraded thermal contact.

Figure 2 exemplary presents the measurement cycles performed on the KETEK SiPM in three different thermal contact configurations. I_{SiPM} is recorded at constant T_{chuck} and V_{bias}, in three time intervals of 320 s each. This time interval is sufficient for reaching thermal equilibrium. The light intensity is set to zero in the first and third intervals, and the dark current, I_{dark}, is measured. In the second interval, the light intensity is set via the current value I_{LED}, previously tuned to induce 25, 50, 75, and 100 mW of dissipated power in the SiPMs. These particular values of dissipated powers are chosen for this study to mimic a non-irradiated SiPM the power observed after neutron irradiation of the HPK SiPM to a fluence $\Phi_{\text{eq}} = 10^{13}$ cm^{-2} operated at −30 °C and 2 V overvoltage. The I-V curves used for this consideration are shown in Figure 3. Compared to a fresh SiPM, the irradiated HPK SiPMs demonstrate an increase in the dark current after irradiation by a factor 10^5 at the excess bias voltage $OV = 2$ V. The same photo-current is induced on a fresh KETEK SiPM by illumination with LED light adjusted to $I_{\text{LED}} = 0.47$ mA, and operating the SiPM at $OV = 10$ V. Other combinations of I_{LED} and OV would also be possible to induce the same power.
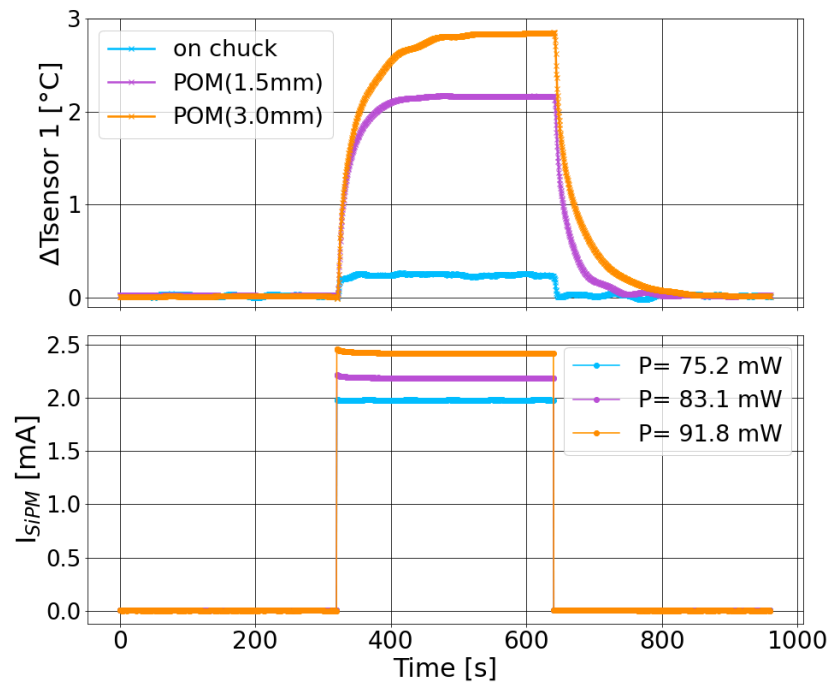
Figure 2. Example of three measurement scan cycles for the KETEK SiPM mounted on alumina (blue) with two POM spacers thicknesses. The temperature change of sensor 1 is plotted versus time (top) and compared to the SiPM current measurement (bottom). The current of the LED is set to zero in the first and third intervals of the cycle. In the second interval, it is switched to a fixed value kept constant for the three cycles. Measurements are taken at 25 °C.
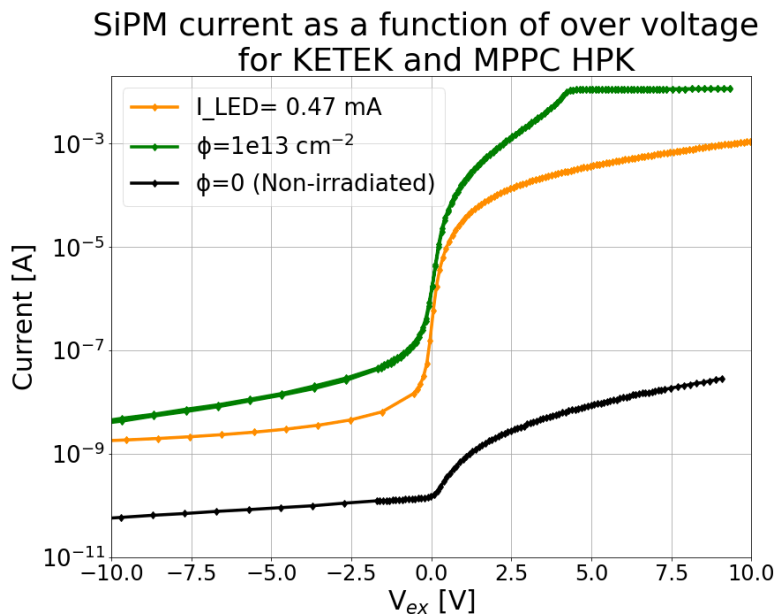

Figure 3. Dark current for a fresh HPK SiPM (black) and the same SiPM irradiated with neutrons at a fluence $\Phi_{eq} = 10^{13}$ cm^{-2} (green), compared to the photocurrent of a fresh KETEK SiPM exposed to LED light. The light intensity is tuned to reach the same range as the irradiated SiPM at an excess bias voltage $OV = 2$ V.

The photo-current is defined as $I_{photo}(I_{LED}) = I_{SiPM}(I_{LED}) - I_{SiPM}(I_{dark})$.

4. Analysis

From the calibration data, $I_{photo}^{cal}(V_{bias}, T_{chuck}, I_{LED})$, the photo-current sensitivity S_{photo} is obtained using the formula:

$$S_{photo}(V_{bias}, T_{chuck}) = \frac{1}{I_{photo}^{cal}} \cdot \frac{dI_{photo}^{cal}}{dV_{bias}} \cdot \frac{dV_{bd}}{dT_{chuck}} \left[\frac{1}{K}\right] \qquad (1)$$

for different I_{LED} values. The sensitivity gives the relative change of I_{photo} for a temperature change of 1 K. In Eq. 1 it is assumed that the sensitivity for a given photon flux I_{photo} only depends on the excess voltage $OV = V_{bias} - V_{bd}(T)$. The sensitivity curves obtained from the calibration data for various LED currents as a function of OV are shown in Figure 4 for KETEK (left) and for HPK (right). The HPK measurements were taken at temperatures of 25 °C and −30 °C. In the range of interest of the measurements, the sensitivity is between 0.004 and 0.01 K^{-1}. As expected, I_{photo} increases with I_{LED} for a constant T_{chuck}, since the current is proportional to the rate of converted photons producing a Geiger discharge (R_γ) and the PDE, $I_{photo} = q_0 \cdot G \cdot R_\gamma \cdot PDE \cdot ECF$ [13]. But it can be seen that S_{photo} does not depend on I_{LED}. Effects of heating and occupancy can be ignored when extracting this calibration function. The T-dependence of the breakdown voltage is derived from the calibration data recorded at different T_{chuck}, yielding to the dV_{bd}/dT values presented in Table 1.
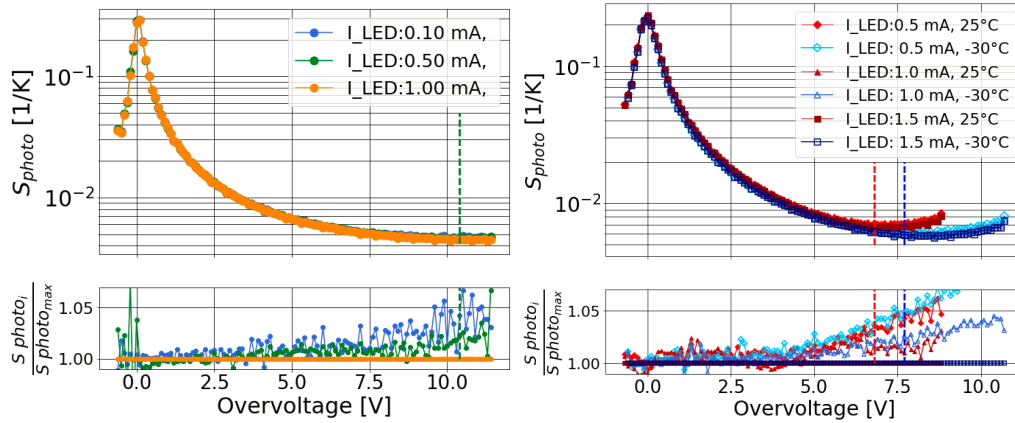

Figure 4. Sensitivity curve at several LED currents for the KETEK sample at 25 °C (left), and for the HPK sample (right). For HPK data with red (blue) symbols are taken at 25 °C (−30 °C). The dashed lines indicate the overvoltages at which the measurement cycles presented in Sec. 5 are taken: $OV = 10.4$ V (KETEK), $OV = 6.8$ V (HPK, 25 °C), and $OV = 7.7$ V (HPK, −30 °C). At the bottom the ratio of sensitivity to the one for the largest I_{LED} are shown.

Once the sensitivity curve is known, the change in SiPM temperature during a measurement cycle (or during operation in an experiment) is calculated from the relative change in photo-current, divided by the sensitivity:

$$\Delta T_{SiPM} = \frac{1}{S_{photo}} \cdot \frac{\Delta I_{photo}}{I_{photo}}, \qquad (2)$$

where $\Delta I_{photo} = I_{photo}(t_1) - I_{photo}(t)$, is defined as the (time-dependent) difference of the photo-current to the first measured value after the LED is switched on. If the time t_1 is sufficiently close to the time of the LED switching, it is assumed that the temperature before and after the switch is still the same. This can be used to impose continuity constraints on the measured temperature profile during a scan. In Figure 5 the temperature changes induced on the SiPM after switching on the LED in the second interval of the cycles reported in Figure 2 are calculated using Eq. 2. The first points of the blue curve show that the main change is in the first step, therefore the assumption of no T change for the first point after the switching on the LED is not completely fulfilled. This may induce the largest error in the calibration of the temperature increase. The temperature of SiPM mounted directly on the

alumina increases only by half a degree, while the SiPMs isolated via POM experience an increase of 3-4 K, depending on the thickness of the substrate.
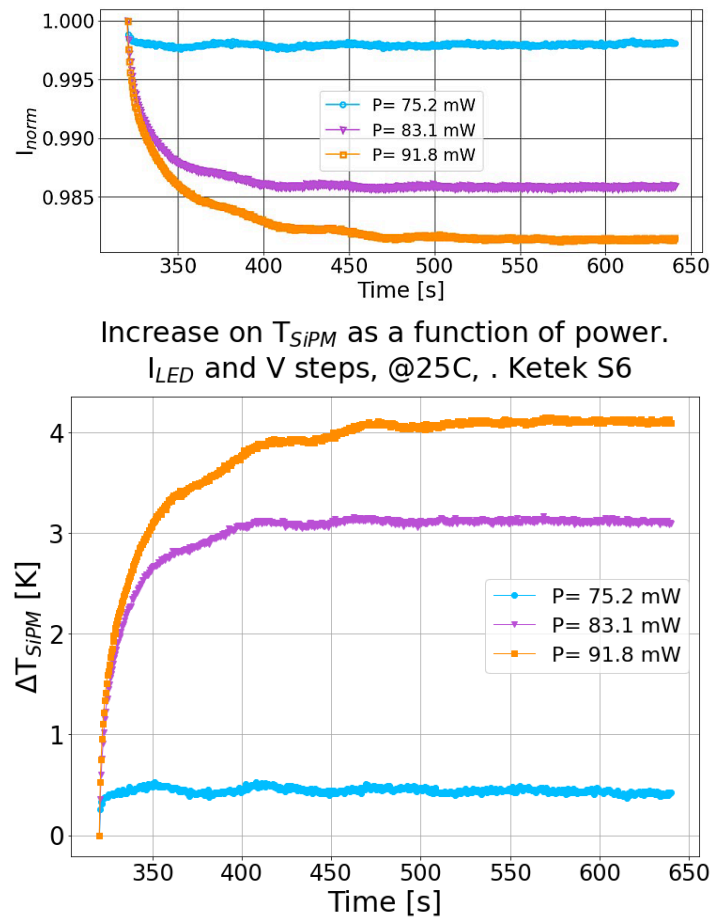

Figure 5. Top) Current of the KETEK SiPM measured at 25 °C in the central interval of the cycles of Figure 2, normalized to the first measurement after the LED switch. The LED light intensity is fixed for the three cycles. The SiPM mounted on alumina thermalizes with a fast time constant, while the SiPM isolated via POM presents a longer thermalization constant. Bottom) Temperature change induced on the SiPM after switching on the LED, calculated using Eq. 2.

The cycle presented in Figure 2 assumes that the SiPM parameters at fixed bias voltage are not instantaneously varied by the increase of light intensity in the second step (B). To evaluate the difference between our assumption and the one applied by Lucchini et al. [14], we performed a second cycle scan, depicted in Figure 6, where the LED intensity is kept fixed and the SiPM bias voltage is changed from a value below to above breakdown, to generate in step B exactly the same power as in the previous cycle.
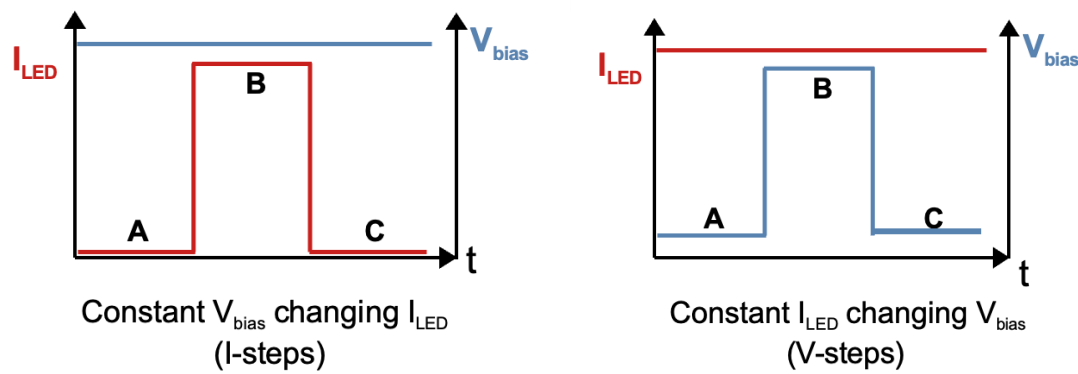
Figure 6. Schematic of the two type of cyles performed to to obtained the results presented in Figure 7. Left) The LED current is stepped from zero to a tuned value and back, while keeping the SiPM bias voltage fixed. Right) The SiPM bias voltage is stepped from 2 V below breakdown to a tuned value and back, while keeping the LED current fixed. The tuned values are such that in step B the power on the SiPM is equal in both cycles.

The the temperature changes induced on the SiPM in step B of both cycles shown in Figure 6, are compared in Figure 7. The values obtained and the temperature gradients are the same for both scans, indicating that the change in SiPM parameters from below to above breakdown do not influence significantly the measurements of self-heating.
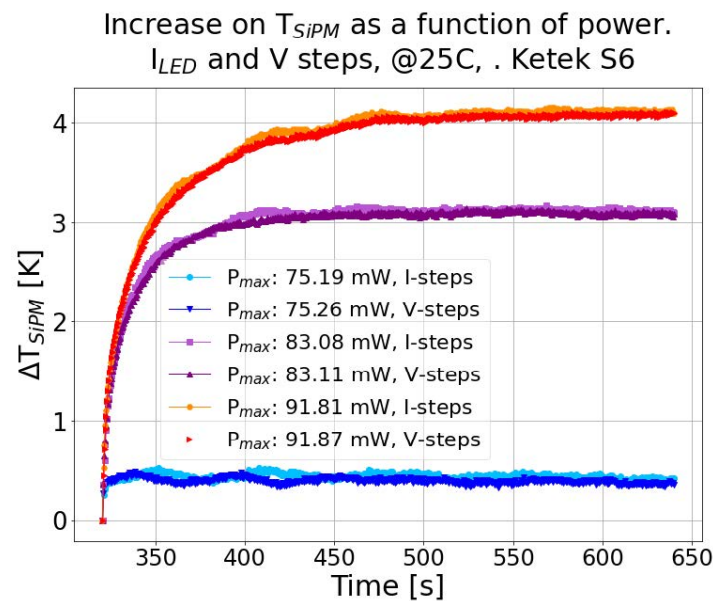

Figure 7. Temperature change induced on the SiPM in step B of the two cycles discussed in Figure 6.

In the following section ΔT_{SiPM} values for long enough times are quoted for which the current has reached a steady state after the switch.

5. Determination of Self-Heating

The procedure described in Sec. 3 and the analysis of Sec. 4 are applied to investigate the two SiPMs under study, described in Table 1. Four LED light intensities are chosen to study the temperature increase of the SiPMs in the relevant power range in the dark expected after irradiation. The value of 50 mW is marked as a reference in the plots, which corresponds to the power of a HPK SiPM irradiated to a fluence $\Phi_{\mathrm{eq}} = 1 \times 10^{13}$ cm^{-2} and operated at $OV = 2$ V and $T = -30\,°$C.

As expected, ΔT_{SiPM} is proportional to the power, as demonstrated in Figure 8, for measurements performed at $T_{\text{chuck}} = 25\,°\text{C}$.
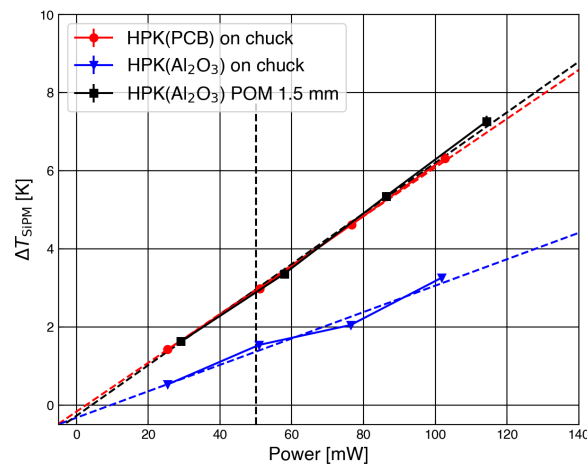

Figure 8. Temperature increase by self-heating as a function of the power dissipated in the SiPM. Best thermal contact is obtained with alumina substrate directly on the chuck (green squares). The thermal contact of the flexible PCB (red circles) shows the same performance as the alumina substrate with 1.5 mm thick POM spacer (green triangles).

The best thermal contact is obtained for the SiPM mounted on the alumina substrate and directly placed on the chuck. In this configuration, the increase in temperature calculated using Eq. 2 is $\Delta T_{\text{SiPM}} = 1.5\,\text{K}$. The 1.5 mm thick POM layer degrades the thermal contact of the SiPM on the alumina substrate to the same level as the flexible PCB. For both configurations $\Delta T_{\text{SiPM}} = 3.0\,\text{K}$. This demonstrates the significant influence of the thermal contact on the self-heating of SiPMs, the better the thermal contact the lower the increase on ΔT_{SiPM}.

Figure 9 compares the results for the two SiPM types investigated: At best thermal contact the minimum temperature increase by self-heating is measured for the KETEK sample, $\Delta T_{\text{SiPM}} = 0.2\,\text{K}$. This value is considerably lower than that obtained for the HPK sample tested in the same condition. This may be attributed to the thermal property of the HPK package, which has a higher thermal resistance than the bare thermal contact compared to the bare KETEK silicon sensor. The same is observed when comparing the temperature increase of HPK on PCB with that of KETEK on alumina plus 1.5 mm thick POM layer, which according to the result shown in Figure 8 should lead to the same thermal increase. The increase of ΔT_{SiPM} is not scaling linearly with the thickness of POM indicating that maybe the thermal coupling via air gap is not ideal or that a more complex volume effect has to be considered. To confirm this effect, detailed 3D finite element simulations of the experimental setup are ultimately required, including the correct boundary conditions.
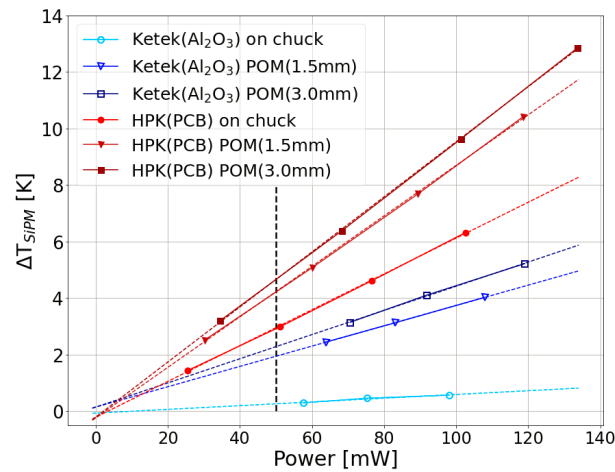
Figure 9. Comparison of temperature increase by self-heating as a function of the power dissipated for two SiPM models: KETEK (blue), and HPK on PCB (red). Circles represent data taken with the substrate on top of the chuck surface, triangles are for data using the thinner POM layer in between, and squares for the thicker POM layer. The dotted lines are linear fits to the data. The vertical dashed line corresponds to the reference power of 50 mW.

Table 2 summarizes the ΔT_{SiPM} values at 50 mW with the corresponding breakdown voltage increase, ΔV_{bd}, which is proportional to the increase in temperature and is determined using the dV_{bd}/dT reported in Table 1.

Table 2. Breakdown voltage and temperature increase by self-heating for KETEK and HPK SiPMs at 25 °C dissipating 50 mW power. The overvoltage during the measurement cycles were $OV = 10.4$ V (KETEK), $OV = 6.8$ V (HPK).

Sample	Substrate	POM [mm]	ΔV_{bd} [mV]	ΔT_{SiPM} [K]
KETEK	Al_2O_3	0	6	0.2
KETEK	Al_2O_3	1.5	44	2.0
HPK	Al_2O_3	0	50	1.5
HPK	Al_2O_3	1.5	100	3.0
HPK	PCB	0	100	3.0
HPK	PCB	1.5	140	4.2
HPK	PCB	3.0	154	4.6

Measurements taken at 25 °C and at −30 °C with the HPK sample soldered on PCB are compared in Figure 10, and analysed using Eq. 2. The results are reported in Figure 11.
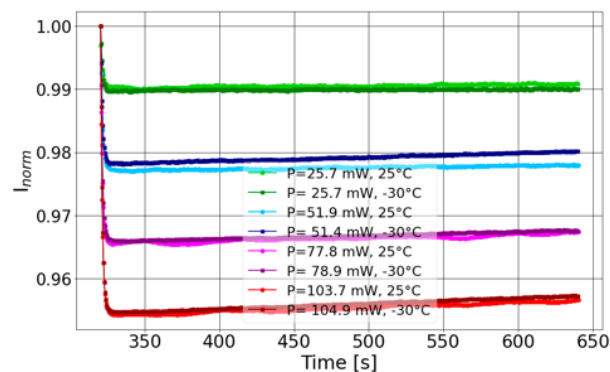

Figure 10. SiPM current measured in step B of the cycle performed with the HPK SiPM at 25 °C and at −30 °C.
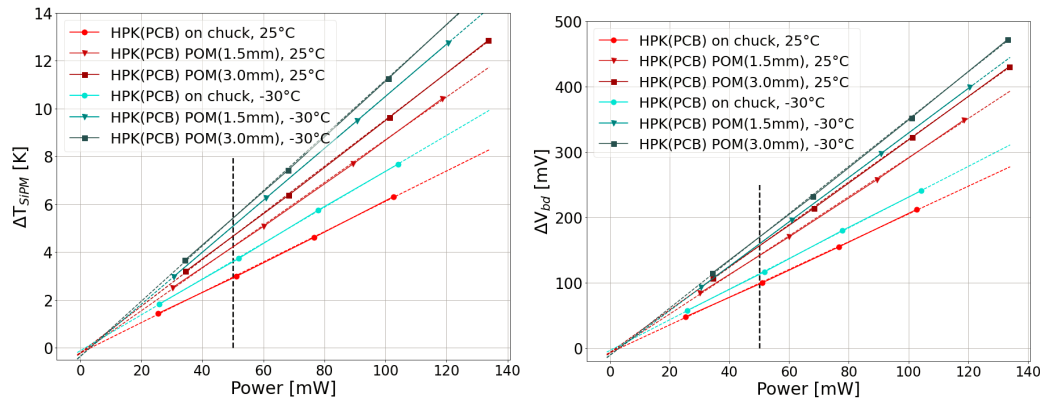
Figure 11. Comparison of temperature increase by self-heating (left) and breakdown voltage shift (right) as a function of the power dissipated for 25 °C (red) and −30 °C (cyan). Circles indicate data taken with the substrate on top of the chuck surface, and triangles (squares) data using the thinner (thicker) POM layer. The dotted lines are linear fits to the data. The vertical dashed line corresponds to 50 mW.

The ΔT_{SiPM} values for 50 mW are summarised in Table 3. The induced temperature increase by self-heating at −30 °C is slightly higher than at 25 °C. While the relative change in current $\left(\frac{\Delta I_{\text{photo}}}{I_{\text{photo}}}\right)$ is the same at high and low temperatures, the sensitivity is at −30 °C ($S_{\text{photo}} = 0.6\,\%/\text{K}$) is lower than at 25 °C ($S_{\text{photo}} = 0.7\,\%/\text{K}$).

Table 3. Breakdown voltage and temperature increase by self-heating HPK SiPM at 25 °C and −30 °C dissipating 50 mWpower. The overvoltage during the measurement cycles were $OV = 6.8$ V (HPK, 25 °C), and $OV = 7.7$ V (HPK, −30 °C).

Sample	Substrate	POM [mm]	T [°C]	ΔV_{bd} [mV]	ΔT_{SiPM} [K]
HPK	PCB	0	25	10	3.0
HPK	PCB	0	-30	113	3.6
HPK	PCB	1.5	25	140	4.2
HPK	PCB	1.5	-30	160	5.1
HPK	PCB	3.0	25	158	4.7
HPK	PCB	3.0	-30	170	5.4

6. Conclusions

A method is developed to determine the self-heating of a SiPM from the measurement of its photo-current. The method is tested as a function of induced power, thermal contact, and two different substrates on two SiPM models with different packages. Self-heating causes an increase in breakdown voltage and a decrease in SiPM photo-current operated at fixed bias voltage. In these measurements, the SiPM is illuminated by a blue LED, and its current transients are measured at constant bias voltage when changing the LED current.

The developed method is used to determine the temperature increase for a SiPM with dissipated power around 50 mW, which is the measured power of an HPK SiPM (MPPC S14160-976X) irradiated to a fluence $\Phi_{\text{eq}} = 1 \times 10^{13}\,\text{cm}^{-2}$ and operated at 2 V above breakdown voltage at −30 °C, taken as reference. For different thermal resistances between the HPK SiPM and the chuck, the following results are obtained: for ideal thermal contact (SiPM on Al_2O_3 substrate) an increase of between 0.2 K and 1.5 K is observed depending on the SiPM package; for realistic thermal contact (SiPM mounted on a PCB), the temperature is larger and ranges between 2 - 3 K, corresponding to an increase in V_{bd} of 50 to 100 mV.

These results demonstrate the importance of a proper investigation of the thermal properties of SiPM package, substrate, and thermal connection to a cooling system when planning to operate at high (dark or photo-) currents. Also, the method proposed in this paper can be used to apply adjustments on the operation voltage depending on the value of the SiPM current during operation.

References

1. Kochanek, I. Packaging strategies for large SiPM-based cryogenic photo-detectors. *Nuclear Instruments and Methods in Physics Research Section A: Accelerators, Spectrometers, Detectors and Associated Equipment* **2020**, *980*, 164487. doi:https://doi.org/10.1016/j.nima.2020.164487.

2. Agishev, R.; Comerón, A.; Bach, J.; Rodriguez, A.; Sicard, M.; Riu, J.; Royo, S. Lidar with SiPM: Some capabilities and limitations in real environment. *Optics & Laser Technology* **2013**, *49*, 86–90. https://doi.org/10.1016/j.optlastec.2012.12.024.

3. Riu, J.; Sicard, M.; Royo, S.; Comerón, A. Silicon photomultiplier detector for atmospheric lidar applications. *Optics Letters* **2012**, *37*, 1229 – 1231. doi:10.1364/OL.37.001229.

4. Garutti, E.; Musienko, Y. Radiation damage of SiPMs. *Nucl. Instrum. Methods Phys. Res. A* **2019**, *926*, 69–84. doi:10.1016/j.nima.2018.10.191.

5. Heering, A.; Musienko, Y.; Ruchti, R.; Wayne, M.; Karneyeu, A.; Postoev, V. Effects of very high radiation on SiPMs. *Nuclear Instruments and Methods in Physics Research Section A: Accelerators, Spectrometers, Detectors and Associated Equipment* **2016**, *824*, 111–114. Frontier Detectors for Frontier Physics: Proceedings of the 13th Pisa Meeting on Advanced Detectors, doi:https://doi.org/10.1016/j.nima.2015.11.037.

6. Contardo, D.; Klute, M.; Mans, J.; Silvestris, L.; Butler, J. Technical Proposal for the Phase-II Upgrade of the CMS Detector. Technical report, Geneva, 2015. doi:10.17181/CERN.VU8I.D59J.

7. CMS Collaboration. The Phase-2 Upgrade of the CMS Endcap Calorimeter. Technical report, CERN, Geneva, 2017. doi:10.17181/CERN.IV8M.1JY2.

8. CMS Collaboration. A MIP Timing Detector for the CMS Phase-2 Upgrade. Technical report, Geneva, 2019.

9. Garutti, E.; Klanner, R.; Lomidze, D.; Schwandt, J.; Zvolsky, M. Characterisation of highly radiation-damaged SiPMs using current measurements, 2017, [arXiv:physics.ins-det/1709.05226].

10. Cerioli, S.; Garutti, E.; Klanner, R.; Martens, S.; Schwandt, J.; Zvolsky, M. Analysis methods for highly radiation-damaged SiPMs. *Nucl. Instrum. Meth. A* **2020**, *958*, 162729, [arXiv:physics.ins-det/1904.07023]. doi:10.1016/j.nima.2019.162729.

11. Musienko, Y.; Heering, A.; Ruchti, R.; Wayne, M.; Andreev, Y.; Karneyeu, A.; Postoev, V. Radiation damage of prototype SiPMs for the CMS HCAL Barrel phase I upgrade. *Nuclear Instruments and Methods in Physics Research Section A: Accelerators, Spectrometers, Detectors and Associated Equipment* **2018**, *912*, 359–362. New Developments In Photodetection 2017, doi:https://doi.org/10.1016/j.nima.2017.12.059.

12. Bornheim, A.; others. Integration of thermo-electric coolers into the CMS MTD SiPM arrays for operation under high neutron fluence. *JINST* **2023**, *18*, P08020, [arXiv:physics.ins-det/2306.00818]. doi:10.1088/1748-0221/18/08/P08020.

13. Klanner, R. Characterisation of SiPMs. *Nucl. Instrum. Methods Phys. Res. A* **2019**, *926*, 36–56. doi:10.1016/j.nima.2018.11.083.

14. Lucchini, M.; Musienko, Y.; Heering, A. Experimental method to monitor temperature stability of SiPMs operating in conditions of extremely high dark count rate. *Nucl. Instrum. Methods Phys. Res. A* **2020**, *977*, 164300. doi:10.1016/j.nima.2020.164300.

15. Garutti, E.; Klanner, R.; Popova, E.; Martens, S.; Schwandt, J.; Villalba, C. Self-heating effect in Silicon-Photomultipliers. *Nucl. Instrum. Methods Phys. Res. A* **2022**, *1039*, 167026. doi:10.1016/j.nima.2022.167026.

16. KETEK GmbH. https://www.ketek.net/, accessed on 2024-01-22.

17. Chmill, V.; Garutti, E.; Klanner, R.; Nitschke, M.; Schwandt, J. Study of the breakdown voltage of SiPMs. *Nucl. Instrum. Meth. A* **2017**, *845*, 56–59, [arXiv:physics.ins-det/1605.01692]. doi:10.1016/j.nima.2016.04.047.

18. Hamamatsu Photonics K.K. https://www.hamamatsu.com, accessed on 2024-01-22.

19. Keithley 6517B electrometer. https://www.tek.com/de/manual/specialty-instruments/keithley-high-resistance-low-current-electr-0-keithley-high-resistance-low-current-electrom, accessed on 2024-01-22.